DESIGN AND IMPLEMENTATION OF THE LLRF SYSTEM FOR LCLS-II*

C. Serrano[†], K. Campbell, L. Doolittle, Q. Du, G. Huang, J. Jones, V. Vytla,
LBNL, Berkeley, CA 94720, USA

S. Babel, A. Benwell, M. Boyes, G. Brown, D. Cha, D.B. Dalit, J. DeLong, J. Diaz-Cruz, B. Hong,
R. Kelly, A. McCollough, M. Petree, A. Ratti, C. Rivetta, SLAC, Menlo Park, CA 94025, USA

R. Bachimanchi, C. Hovater, D. Seidman, JLab, Newport News, VA 23606, USA

B. Chase, E. Cullerton, J. Einstein, J. Holzbauer, D. Klepec, Y. Pischalnikov, W. Schappert,
Batavia, IL 60555, USA

ABSTRACT

The SLAC National Accelerator Laboratory is building
LCLS-II, a new 4 GeV CW superconducting (SCRF) Linac
as a major upgrade of the existing LCLS. The SCRF Linac
consists of 35 ILC style cryomodules (eight cavities each)
for a total of 280 cavities. Expected cavity gradients are 16
MV/m with a loaded Q_L of $\sim 4 \cdot 10^7$. Each individual RF
cavity will be powered by one 3.8 kW solid state amplifier.
To ensure optimum field stability a single source single cavity
control system has been chosen. It consists of a precision
four channel cavity receiver and two RF stations (Forward,
Reflected and Drive signals) each controlling two cavities.
In order to regulate the resonant frequency variations of
the cavities due to He pressure, the tuning of each cavity is
controlled by a Piezo actuator and a slow stepper motor. In
addition the system (LLRF-amplifier-cavity) was modeled
and cavity microphonic testing has started. This paper will
describe the main system elements as well as test results on
LCLS-II cryomodules.

INTRODUCTION

LCLS-II is an X-ray Free Electron Laser (FEL) under construction at SLAC, driven by a superconducting RF Linac [1].
The electron beam quality will directly translate to the quality of the X-ray beams produced in undulators and used for
scientific research in the end stations; hence strict requirements have been placed on the stability of the accelerating
cavity fields. An initial stability goal of 0.01° in phase and
0.01% amplitude has been set for the main Linac, composed
of 280 nine-cell 1300 MHz superconducting cavities [2].

Plans for the RF controls for the 1.3 GHz cavities have
been described elsewhere ([3–6]). It is based on mainstream
digital LLRF technology, and incorporates many ideas developed for LBNL's NGLS proposal [7]. The controls use
a Single Source Single Cavity (SSSC) architecture, where
each cavity has a dedicated amplifier. SSSC has enormous
value for simplifying control of narrow-band SRF cavities, It
is also a sensible choice for a CW machine, where Solid-State
Amplifier technology has approximately matched Klystrons
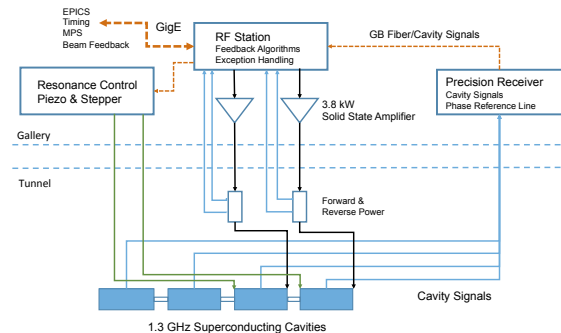

Figure 1: System hardware configuration supporting half of
a cryomodule (one of two RF Station chassis shown).

in price, and they are considered easier to operate and maintain.

The LLRF subsystem of LCLS-II is itself a four-laboratory
collaboration: LBNL for architecture, FPGA hardware and
RF DSP programming, and ADC/DAC hardware development; FNAL for downconverters, upconverters and piezo
drivers; JLab for interlocks, stepper controls, and power supplies; and SLAC for LO distribution, MO and PRL, global
control system integration, commissioning, transition to operations, and project management.

SYSTEM DESIGN

Each rack (supporting four cavities) includes a separate
Precision Receiver Chassis (PRC), linked only by optical
fiber to two RF Control Chassis (RFS), as shown in Fig. 1.
This density of rack equipment matches the civil layout of
the accelerator, where one LLRF rack is cabled to one penetration to the tunnel. The physical separation between PRC
and RFS maximizes isolation between the critical stabilized
cavity signals and the wildly fluctuating forward and reverse
monitoring channels. Preliminary measurements show that
this separation has succeeded, in that the measured isolation
is at least 125 dB.

The system bypasses some of the usual compromises in
choosing an IF by means of an unusual split-LO design,
where a low-frequency IF (20 MHz) is used for RF downconversion, and a higher-frequency IF (145 MHz) is used for
RF upconversion. Separating transmit and receive signals in

Figure 2: 1.3 GHz downconverter block diagram.

Figure 3: Chassis differential phase noise power spectral density at 1300 MHz.

the frequency domain has the added advantage of removing a perennial source of crosstalk from the drive back to RF inputs.

LOW NOISE ANALOG/RF DESIGN

An RF Downconverter circuit board uses a 1320 MHz LO, distributed to each of the racks, to generate a 20 MHz IF for digitization. This board uses careful RF design and to achieve typically -90 dB channel-channel crosstalk. It also acts as an LO distribution module for the chassis.

Downconverter

The 6-channel precision receiver is an RF board designed to convert 1.3 GHz RF signals to 20 MHz IF signals for digital signal processing. To minimize channel to channel isolation, the board receives RF signals using Type-N connectors bolted through the rear panel into a shielding enclosure, providing a continuously enclosed path to the RF section of the board. The Type-N connections bolted through the rear-panel also provide a rugged connection to RF signals arriving over 3/8" heliax cable. Other design features to improve isolation include the selection a mixer with high RF-LO isolation, an amplifier and an attenuator driving the LO port of each mixer, and high isolation splitters in the LO distribution section. To design for maximum linearity, a mixer and IF amplifier with a high IP3 were selected. Careful placement of attenuators around the mixer is required to balance the linearity and output noise floor. Selection of a good low noise IF amplifier minimized the noise floor at the IF output.

Upconverter

The 2-Channel Upconverter is an RF board designed to convert 145 MHz IF signals from the DAC's of the LLRF digital signal processor to 1.3 GHz RF signals for driving LCLS-II cavities. Several design choices were made to minimize spurious signals at the RF output, choosing an IF frequency of 145 MHz and a LO frequency of 1155 MHz to maximize LO carrier and RF frequency separation. A single sideband IQ modulator was used to reduce spurious signals, which has a high carrier and sideband suppression.

To achieve channel to channel isolation better than 60 dB without shielding, the spacing between channels was maximized. A transmission line was also designed to reduce radiation and via walls were placed around the transmission lines. Filtering of common lines to both channels was also required to maintain isolation between channels. Common lines include power supplies and RF switch circuitry. Shielding was added to the board to reduce the channel to channel isolation to 70 dB. The shielding also reduced the amount of spurious coupling.

The output noise was minimized by using a center tapped balun to convert the single ended I and Q signals to differential signals at the input of the IQ modulator instead of a using a single ended to differential amplifier, which usually contributes a significant amount of noise to the circuit. A low noise IF amplifier was used to amplify the single ended IF signal before the balun, and a low noise reference voltage was used at the center tap of the balun to provide the common mode DC offset required by the IQ modulator. To maintain good linearity from the IF input to the RF output, high IP3 IF and RF amplifiers were used, along with proper balance of attenuators throughout the signal chain.

Chassis Integration

Both the digitizer and RF downconversion hardware are mounted on a 6 mm aluminum plate to keep their component temperatures stable. They also both use low-noise LDO voltage regulators to avoid injecting noise from power supplies into the signal path. Those low-noise regulators use a capacitor to filter the voltage reference at audio frequencies; non-piezoelectric capacitors are used to avoid picking up environmental mechanical noise (e.g., fans).

Differential phase noise of a completed RF chassis was measured using a 1300 MHz source passively split to two input channels. After digital downconversion, filtering, and decimation, long data traces were saved for analysis. One such resulting differential phase noise power spectrum den-
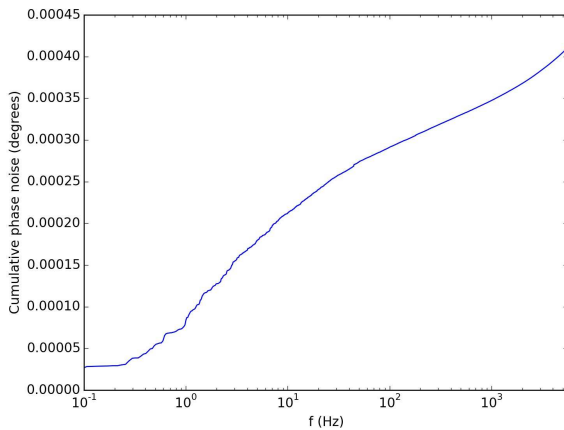
Figure 4: Chassis cumulative differential phase noise.

sity plot is shown in Fig. 3. Between $1/f$ and white noise, power integrals diverge for both low and high frequencies.

The final use case with beam-based feedback running (see below) will effectively apply a 1 Hz high-pass filter to this noise; therefore this measured noise can have such a filter applied to it. That curve's low-frequency integral then converges, so it's legitimate to plot the cumulative noise starting at DC. Such a plot is shown in Fig. 4.

TESTING

Prototype LCLS-II cryomodules are in testing at FNAL and JLab, and prototypes of the RF control system have also been installed there. A photo of one such LCLS-II rack is shown in Fig. 5. This rack will control and monitor four cavities; it includes three RF chassis, each with six 1300 MHz inputs. Each test facility also has its own set of RF controls; RF splitters have been installed on each cavity's forward, reverse, and probe ports, so that both controllers can simultaneously monitor the state of the cavity. This situation is ideal for development and debugging, including the ability to make out-of-loop measurements.

We have demonstrated automated routines running on a general-purpose computer (connected by Ethernet to the rack of FPGAs) bringing a cavity on from scratch. By setting up and analyzing pulsed waveforms, the routines measure such properties as the cavity bandwidth, resonance frequency, SEL phase offset, and plant gain.

This gives one-button turn-on to CW closed-loop operation. SEL capabilities allow centering the cavity tune (at the operational gradient) to be considered as a leisurely second step.

Figures 6 through 8 show the digital SEL switching in and out of resonance tracking mode; these data were taken at a time when the cavity static tuning was slightly off. In 0.3 seconds, the system briefly entered resonance-tracking mode six times. The largest phase deviation of the cavity during any of these times was 7.3°. The apparent overshoot and non-ideal transitions between phase-locked and resonance-

Figure 5: Prototype Chassis installed at the FNAL CMTS.

tracking "modes" (really determined by whether or not the imaginary drive terms has clipped) are an artifact of the waveform recording. That recording only has a bandwidth of 2.8 kHz, but the transitions happen on the 1 μs time scale. Note that the cavity gradient stays completely fixed during this time, because the amplitude loop continues to operate. Constant field amplitude gives constant Lorentz forces, and therefore no internal excitation of detuning excursions.

The locus of forward drive complex numbers shown in Fig. 7 nicely shows the vertical line understood by resonance theory for a fixed cavity vector. Once the imaginary part of the drive reaches its clipping threshold, the phase moves freely, and and the locus follows a fixed radius circle.

In-loop phase error measurements are effectively zero, 0.00013° RMS over the frequency band 0.1 Hz to 2.8 kHz, while the feedback was generating reactive drive for microphonics suppression of 4.4° RMS.

Out-of-loop phase error measurements were taken by the FNAL LLRF system measuring in parallel. Those results are shown in Fig. 9; the overall phase error is 0.0016° RMS over the frequency band 0.1 Hz to 5.0 kHz. A cumulative
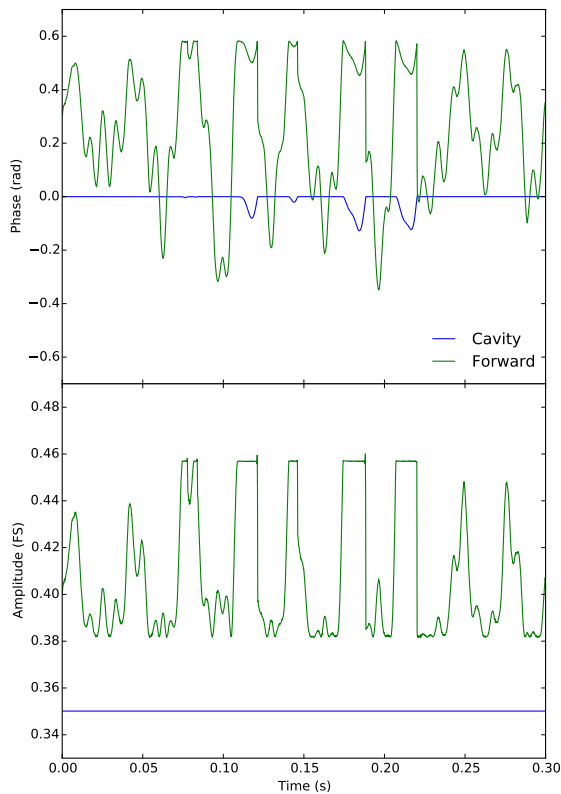
THSH202

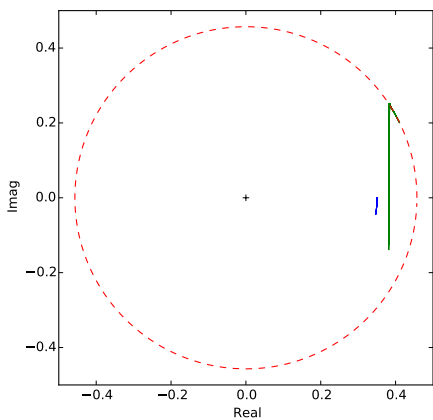Figure 6: SEL operations with ordinary time axes.

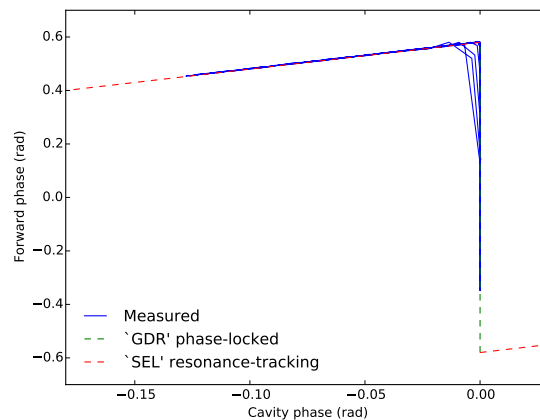Figure 7: Locus of SEL operations in the complex plane.

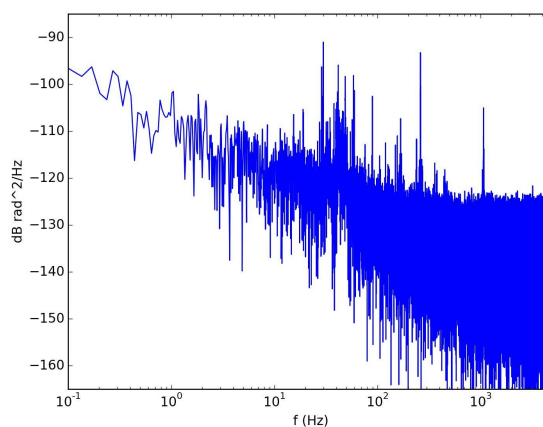Figure 8: Connection between cavity and drive phase during SEL operations

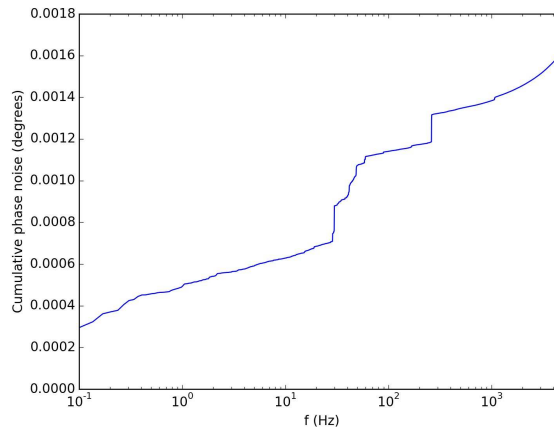

Figure 9: Out-of-loop phase noise power spectrum density.
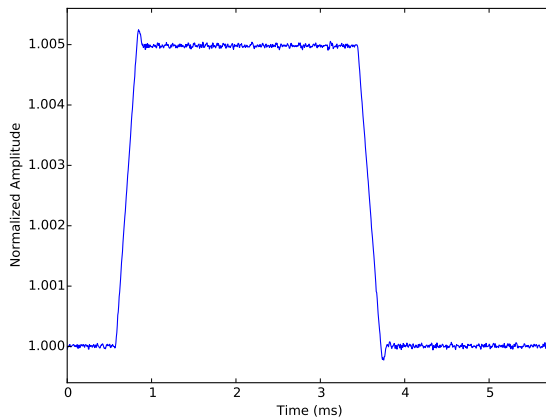

Figure 10: Out-of-loop cumulative phase noise.

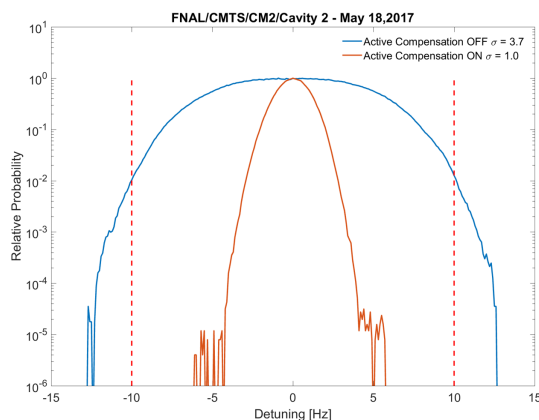Figure 11: Amplitude loop response to 0.5% setpoint modulation.

Figure 12: Effect of active resonance compensation on cavity detuning. Experiment performed on Cryomodule 2 at the FNAL test stand.

plot, integrated up from 0.003 Hz, is shown in Fig. 10. The FNAL data acquisition system has larger white noise and crosstalk than the LCLS-II system, and similar $1/f$ noise. Consequently, this measurement should be considered an upper limit, and the actual performance of the LCLS-II system is better than this to a level still to be determined. It's possible to extrapolate some bench measurements to a cavity run at -5 dBFS, to get 0.0005° RMS above 1 Hz for a 20 kHz closed-loop bandwidth, but that is not verified.

Actual cavity field variations in the final accelerator will necessarily be larger than the noises quoted above. Cable length variations (including those inside the cryomodule), beam loading, phase reference line contributions, and the ever-elusive unknown unknowns will add to the system errors. The system stability and transient response was checked for a large number of P and I gain settings, known as a gain scan. Figure 11 shows one such response.

RESONANCE CONTROL

LCLS-II baseline calls for development and implementation of active resonance stabilization using the piezo fast tuners. Techniques for active stabilization have been developed at FNAL [8,9] and center around inclusion of the cavity electromechanical system information into the compensation drive. These techniques will be transferred into the existing LCLS-II LLRF hardware for use at the cryomodule test stands at FNAL and JLab as well as machine operation at SLAC.

The compensation technique centers on a set of digital, narrow bandpass filters. The streaming detuning signal is passed through these filters, gain/phase adjusted, then summed and sent to the piezo tuners. The number, center frequency, and width of these filters is set by an optimization routine that includes background (uncompensated) detuning spectra, the piezo/detuning transfer function, and digital hardware limitations. Manual adjustment of the filter parameters has already demonstrated an improvement of over a factor of 3 on an LCLS-II cavity during cryomodule test.

These techniques have been developed and tested using a FPGA-based digital RF system at FNAL. This system include digital up/down converters, on-line detuning calculation, compensation firmware, and other diagnostics. The LCLS-II system already includes most of this functionality, so only the compensation firmware is being adapted to fit with the existing architecture. This work is well underway, with the goal of demonstrating 1-cavity compensation on an upcoming cryomodule test. The goal is to demonstrate a fully automated characterization and compensation routine for an 8-cavity cryomodule.

PLANS

With clear evidence from cryogenic cavity tests that the prototype LCLS-II LLRF system meets critical performance specifications, the system is ready for its Final Design Review. The system's production and installation will follow shortly thereafter. SLAC will lead that effort, with support from the other collaborating laboratories. During the system's checkout and commissioning phase, the technical responsibilities of each lab within in the collaboration will be migrated to SLAC via a Lead, Mentor, and Consult transition plan. LCLS-II as a whole may not achieve final performance goals until some time after first light and the transition to operations. LLRF performance optimization and software maturation will continue as the operating beam current increases and performance expectations rise.

REFERENCES

[1] P. Emma, *et al.* "Linear accelerator design for the LCLS-II FEL facility", in *Proc. FEL'14*, Basel, Switzerland, Aug. 2014, pp 743–747.

[2] P. Emma "LCLS-II Physics requirement document: Linac requirements", SLAC, Menlo Park, CA, USA, Document no. LCLSII-2.4-PR-0041-R2.

[3] C. Hovater and L. Doolittle, "The LCLS-II LLRF system", in *Proc. IPAC'15*, Richmond, VA, USA, 2015, pp 1195–1197.

[4] L. Doolittle, "Analog-centered LLRF system design for LCLS-II", presented at the Low Level Radio Frequency Workshop 2015 (LLRF'15), Shanghai, China, Oct. 2015.

[5] G. Huang *et al.* "High precision RF control for the LCLS-II", in *Proc. NA-PAC'16*, Chicago, IL, USA, Oct. 2016, pp 1292–1296, doi:10.18429/JACoW-NAPAC2016-FRA2IO02

[6] L. Doolittle *et al.* "LLRF control of high Q_L cavities for the LCLS-II", in *Proc. IPAC'16*, Busan, Korea, May 2016, pp 2765–2767, doi:10.18429/JACoW-IPAC2016-WEPOR042

[7] L. Doolittle, A. Ratti, *et al.* "Design of RF controls for precision CW SRF light sources", presented at the Low Level Radio Frequency Workshop 2013 (LLRF'13), Lake Tahoe, CA, Oct. 2013.

[8] W. Schappert *et al.*. "Adaptive Lorentz Force Detuning Compensation in the ILC S1-G Cryomodule at KEK," in *RF Superconductivity (SRF'11)*, Chicago, IL, USA, Jul. 2011, pp 254–257.

[9] W. Schappert, Y. Pischalnikov, and M. Scorrano, "Resonance control in SRF cavities at FNAL," in *Proc. PAC'11*, New York, NY, USA, Mar. 2011, pp. 2130–2132.